



CHALMERS
UNIVERSITY OF TECHNOLOGY

Effect of chemical segregation on accuracy of local lattice distortions determination by pair distribution functions

Downloaded from: <https://research.chalmers.se>, 2024-12-20 12:42 UTC





Citation for the original published paper (version of record):

Hu, Y., Guo, S., Hörnqvist Colliander, M. (2024). Effect of chemical segregation on accuracy of local lattice distortions determination by pair distribution functions. *AIP Advances*, 14(11). <http://dx.doi.org/10.1063/5.0234652>

N.B. When citing this work, cite the original published paper.

RESEARCH ARTICLE | NOVEMBER 06 2024

Effect of chemical segregation on accuracy of local lattice distortions determination by pair distribution functions

Yao Hu (胡尧) ; Sheng Guo ; Magnus Hörnqvist Colliander  

AIP Advances 14, 115310 (2024)

<https://doi.org/10.1063/5.0234652>

Articles You May Be Interested In

Effect of alloying elements on the structure and mechanical properties of NbMoTaWX (X = Cr, V, Ti, Zr, and Hf) refractory high-entropy alloys

AIP Advances (February 2021)

First-principles calculation of phase stability and elastic properties of Cr_xMoNbTiV refractory high-entropy alloys

AIP Advances (September 2023)

Unveiling the interactions between preexisting dislocations and displacement cascades in the refractory high-entropy alloy WTaCrV

J. Appl. Phys. (November 2024)

22 November 2024 13:45:27

AIP Advances

Why Publish With Us?



19 DAYS
average time
to 1st decision



500+ VIEWS
per article (average)



INCLUSIVE
scope

[Learn More](#)

Effect of chemical segregation on accuracy of local lattice distortions determination by pair distribution functions

Cite as: AIP Advances 14, 115310 (2024); doi: 10.1063/5.0234652

Submitted: 27 August 2024 • Accepted: 23 October 2024 •

Published Online: 6 November 2024



View Online



Export Citation



CrossMark

Yao Hu (胡尧),¹  Sheng Guo,²  and Magnus Hörnqvist Colliander^{1,a)} 

AFFILIATIONS

¹Department of Physics, Chalmers University of Technology, Göteborg 41296, Sweden

²Department of Industrial and Materials Science, Chalmers University of Technology, Göteborg 41296, Sweden

^{a)}Author to whom correspondence should be addressed: magnus.colliander@chalmers.se

ABSTRACT

Local lattice distortion (LLD) is a salient feature of bcc-structured refractory high-entropy alloys (RHEAs), closely associated with their mechanical properties. To quantify the extent of LLDs in RHEAs, the pair distribution function (PDF) analysis has been identified as a promising approach. However, the commonly observed chemical segregation within these alloys introduces challenges in accurately determining LLDs. In this study, the effect of chemical segregation on LLD quantification was investigated through fitting simulated two-phase composite PDFs, representing segregated microstructures, with a single-phase model and evaluating the errors to assess the accuracy and reliability of small-box analysis in this context. The results show that the errors introduced by chemical segregation increase with increasing lattice parameter difference, and the fitting quality gradually deteriorates to a point where it no longer adequately describes the data. We found that the lattice parameter difference should be below 1% for precise and reliable LLD measurements in bcc-structured RHEAs. Additionally, we observed that while the scattering length variation due to segregation does affect LLD quantification, its effect is comparatively minor.

© 2024 Author(s). All article content, except where otherwise noted, is licensed under a Creative Commons Attribution (CC BY) license (<http://creativecommons.org/licenses/by/4.0/>). <https://doi.org/10.1063/5.0234652>

Since the concept of high-entropy alloys (HEAs) was first proposed,^{1,2} this innovative material design strategy has significantly impacted both structural^{3–5} and functional materials^{6–8} due to their unique compositional flexibility that allows for tailored properties. Refractory high-entropy alloys (RHEAs), a promising subgroup of HEAs, exhibit high strength at elevated temperatures, making them ideal for advanced structural materials required in extreme conditions, such as jet-turbine engines. The high strength feature has partly been ascribed to the existence of local lattice distortion (LLD), which has also been identified as a crucial factor influencing mechanical properties through solid solution strengthening^{9–11} and a contributor to the stabilization of the body-centered cubic (bcc) phase.¹² Nevertheless, a comprehensive and quantitative understanding of LLDs is still lacking due to the absence of widely accepted measurement techniques and analysis methods.

One of the potential techniques in quantifying LLDs is the use of pair distribution functions (PDFs). PDFs have been suggested as a valuable tool for providing a unique perspective in probing the

local structure of crystalline materials.¹³ Previously, researchers have demonstrated the potential of PDFs for quantitatively characterizing LLDs, particularly through the analysis of peak widths.^{11,14–16} However, this approach can be negatively influenced by factors such as relative scattering lengths, magnitudes of form factors, and correlated motion.¹⁷ These factors can introduce substantial errors in the measurements and potentially complicate the accurate quantification of LLDs. An alternative methodology is to extract atomic displacements through comprehensive fitting of PDFs across an extended r -range.¹⁸ This method may offer a more precise approach to quantify LLDs in various materials.

In order to accurately quantify LLDs in RHEAs, it is essential to also consider the microstructural characteristics of these materials. Several studies have shown that elemental segregation in HEAs is indeed a significant factor.^{19–22} These studies highlight the commonly observed formation of dendritic microstructures in as-solidified HEAs, which can be attributed to the alloys' compositional complexity and the varying melting temperatures of the constituent

elements.⁵ While a segregated microstructure is characterized by continuous variations of the chemistry, it results in the emergence of distinctive regions, such as dendritic and interdendritic regions. As the difference in average lattice parameter is typically relatively small, the contributions from the different regions are difficult to separate. However, as the presence of varying lattice parameters will cause additional broadening of the PDF peaks, segregation can potentially introduce errors in determining LLDs.

Notably, bcc-structured RHEAs have been reported to exhibit higher levels of LLDs compared to their face-centered cubic (fcc) counterparts.^{23,24} This distinction leads us to concentrate primarily on bcc-structured RHEAs in this study. In a previous study,²⁵ we used single-phase fitting of simulated composite PDFs to show that for a specific alloy (HfNbTaTiZr) with a dendritic solidification structure, the effect of segregation on the determination of the LLDs was negligible. However, this conclusion is only valid for the specific combination of lattice parameter difference, LLD magnitude, and elemental distribution investigated in HfNbTaTiZr. For a more general assessment of the error associated with single-phase fitting of segregated RHEAs, and importantly, the corresponding validity of the derived values of the LLDs, a broader range of alloys must be investigated. Experimentally, this is a difficult task as the true LLDs are unknown. On the other hand, the use of simulated PDFs allows the effects of known LLDs to be included along with both certain material related parameters (difference in chemistry and lattice parameter between regions) and instrumental contributions.

To investigate the impact of an inhomogeneous structure on the accuracy of PDF-based LLD determination, we conduct a simulation study covering a broad range of composite PDFs for bcc-structured RHEAs, designed to emulate chemically segregated microstructures. The width of the peaks in a PDF is a convolution of thermal vibrations and static displacements (LLDs). Different atoms experience different static displacements from the ideal positions in the lattice, and each atom vibrates around its displaced position. The combination of static and dynamic displacements leads to a larger variation in the distance between neighboring atoms (i.e., a wider distribution of bond lengths), whereas the average bond lengths are unaffected. Indeed, *ab initio* studies have shown that the distribution of bond lengths is significantly broadened in HEAs, while the average bond length agrees with that calculated from the lattice parameter.¹⁵ Furthermore, the broadening is more pronounced in bcc-structured HEAs compared to their fcc-structured counterparts.²³

To a first approximation, the distributions of both static and dynamic displacements are Gaussian, with standard deviations σ_s and σ_t , respectively. In scattering experiments, the combined effect of these displacements is captured by the derived isotropic displacement parameter U_{iso} , including both static (U_s) and thermal (U_t) components,

$$U_{\text{iso}} = U_s + U_t = \sigma_s^2 + \sigma_t^2. \quad (1)$$

Specifically, in real-space PDFs, an increase in U_{iso} due to the presence of off-site displacements leads to an increase in the peak width $\sigma(r)$, as shown in Fig. 1. This phenomenon is mathematically modeled as^{26,27}

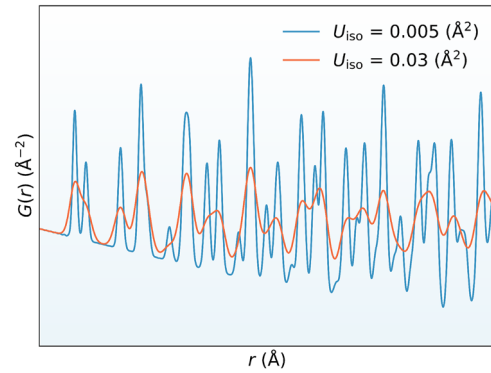


FIG. 1. Broadening PDF peaks with larger U_{iso} values.

$$\sigma(r) = \sqrt{U_{\text{iso}} \left(1 - \frac{\delta_1}{r} - \frac{\delta_2}{r^2} + Q_{\text{broad}}^2 r^2 \right)}, \quad (2)$$

where δ_1 and δ_2 are correction factors for peak narrowing at small r values, addressing the effects of correlated motion. The term Q_{broad} accounts for peak broadening from increased intensity noise at high Q , often only significant for wide r -ranges.

Taking advantage of this characteristic, LLDs can be quantified in terms of the *local lattice strain* (ϵ), expressed as the standard deviation of the static displacements (σ_s) relative to a reference length, often taken as the average atomic radius (\bar{r}),¹⁸

$$\epsilon = \frac{\sigma_s}{\bar{r}}, \quad (3)$$

where $\bar{r} = \frac{\sqrt{3}}{4}a$ according to the hard-sphere model for the bcc structure, and a is the lattice parameter. With $U_s = \sigma_s^2$, Eq. (3) can be written as

$$\epsilon = \frac{\sqrt{U_s}}{\bar{r}}. \quad (4)$$

In a segregated, dendritic microstructure, the boundary between the dendrites and interdendritic regions is not chemically sharp. Instead, it is characterized by continuous modulations in chemical composition. However, for simplicity, we consider it as comprising two distinct “phases”: dendrites (D) and interdendritic regions (ID). Each phase has a different average chemical composition and, as a result, a distinct lattice parameter. The PDF of a multiphase system can be mathematically represented as a weighted sum of the individual PDFs of each phase, as derived by Sławiński,²⁸

$$G(r) = \sum_p w_p G_p(r), \quad (5)$$

where w_p is the weight and $G_p(r)$ is the PDF of phase p . Note that $G(r)$ refers to the *reduced* PDF, which is the function implemented in the DiffPy-CMI framework used in this study. This function is referred to as $G^{\text{PDF}}(r)$ by Sławiński,²⁸ and for this function the scale factors in Eq. (6) are valid. It should not be confused with the *total* PDF, which is often also referred to as $G(r)$.²⁹ We refer to, e.g.,

TABLE I. Parameters for PDF simulation and fitting.

Parameter	Value
Q_{broad}	0.0332
Q_{damp}	0.0311
δ_1	0
δ_2	2.8710
$Q_{\text{min}} (\text{\AA}^{-1})$	0.5
$Q_{\text{max}} (\text{\AA}^{-1})$	34

Peterson and Keen³⁰ for a more detailed discussion on the relationship between the two functions. The weight for each phase is calculated using the formula

$$w_p = x_p \frac{\bar{b}_p^2}{\sum_p x_p \bar{b}_p^2}. \quad (6)$$

In this expression, x_p refers to the molar fraction of phase p , and \bar{b}_p is the average scattering length for that phase,

$$\bar{b}_p = \sum_i c_{i,p} b_{i,p}. \quad (7)$$

Here, $c_{i,p}$ represents the concentration, and $b_{i,p}$ is the scattering length of element i in phase p .

The individual PDFs were simulated with the *PDFCalculator* module in DiffPy-CMI,²⁷ where each phase was defined by the values of U_{iso} , the lattice parameter a , and space group $Im\bar{3}m$. Instrumental effects were accounted for through parameters obtained from a neutron total scattering measurement of pure Nb.²⁵ The correlated motion effects were simulated using δ_2 (with δ_1 set to 0), as it provides a better description of the correlated motion at lower temperatures, as proposed by Jeong *et al.*³¹ All parameters are listed in Table I. We assume that the level of LLDs (U_s) is the same in both the dendrites and interdendritic regions. This assumption can be justified since the actual differences in regions that are chemically similar and structurally identical should be minimal, and minor variations in U_s should not have a significant impact on the PDF.

Each composite PDF was then fitted with a single-phase model in DiffPy-CMI. The fitting range was set to be $1.5 \leq r \leq 20 \text{ \AA}$, as the fitting has been shown to be robust against artifacts in this range,^{32–36} and it is hence the region that should be considered in the fitting of actual experimental data. During this process, only a and U_{iso} were varied. The final parameters from the fit, a_{fit} and $U_{\text{iso}}^{\text{fit}}$, were then used to estimate the LLD using the following equation:

$$\varepsilon_{\text{fit}} = \frac{\sqrt{U_s^{\text{fit}}}}{r_{\text{fit}}} = \frac{\sqrt{U_{\text{iso}}^{\text{fit}} - U_t}}{a_{\text{fit}} \times \frac{\sqrt{3}}{4}}. \quad (8)$$

This estimated strain was then compared with the actual local lattice strain in the simulated structure (ε_{sim})

$$\varepsilon_{\text{sim}} = \frac{\sqrt{U_s^{\text{sim}}}}{\bar{r}_{\text{sim}}} = \frac{\sqrt{U_{\text{iso}}^{\text{sim}} - U_t}}{\bar{a}_{\text{sim}} \times \frac{\sqrt{3}}{4}}. \quad (9)$$

Here, \bar{a}_{sim} , representing the average lattice parameter of the two-phase structure, is calculated as a molar fraction-weighted average of the lattice parameters of the two phases,

$$\bar{a}_{\text{sim}} = (1 - x_{\text{ID}}) \times a_{\text{D}} + x_{\text{ID}} \times a_{\text{ID}}, \quad (10)$$

where x_{ID} is the molar fraction of interdendritic regions. It is important to note that the exact value of the lattice parameter only has a minimal effect on the result. We quantified the relative difference between the fitted and true LLD using the following error measure:

$$\eta = \frac{|\varepsilon_{\text{fit}} - \varepsilon_{\text{sim}}|}{\varepsilon_{\text{sim}}}, \quad (11)$$

which effectively captures the extent of error introduced by applying a single-phase model to a segregated system. The procedure is outlined schematically in graphical form in the [supplementary material](#).

First, we investigate how the difference in lattice parameter between the regions and their respective molar fractions impacts the accuracy of the LLDs derived from single-phase fits of the simulated composite PDFs. To isolate these effects, we initially assume a negligible difference in average scattering length between the regions, i.e., $b_{\text{D}} = \bar{b}_{\text{ID}}$.

In the simulations, the lattice parameter of one phase, a_{D} , was kept constant at 3.4 \AA , while the lattice parameter of the second phase was varied from in the range $a_{\text{D}} \leq a_{\text{ID}} \leq 1.03a_{\text{D}}$ (i.e., a maximum difference of 3% based on reported lattice parameter differences from the literature; see Table II). For each value of the lattice parameter difference (hereafter denoted by $\Delta a = |a_{\text{ID}} - a_{\text{D}}|/a_{\text{D}}$), we varied the static displacements, U_s^{sim} from 0 to 0.025 \AA^2 (i.e., U_{iso} varied between 0.005 and 0.03 \AA^2 , assuming a typical thermal component, $U_t^{\text{sim}} = 0.005 \text{ \AA}^2$ based on previous results from HfNbTaTiZr²⁵).

Figure 2(a) shows the resulting composite PDFs corresponding to the extreme cases for $x_{\text{ID}} = 0.5$. Clearly, the presence of segregation ($\Delta a \neq 0$) has a pronounced effect on the PDFs, and the effect increases rapidly with r . Fitting the composite PDFs with large lattice parameter differences with a single-phase model results in significant deviations from the model, as shown in Figs. 2(b) and 2(c). In particular, the combination of large lattice parameter differences and

TABLE II. Reported lattice parameters and their differences in some segregated bcc-structured RHEAs.

Alloy	$a_1 (\text{\AA})$	$a_2 (\text{\AA})$	$\Delta a (\%)$	References
HfNbTaTiZr	3.397	3.4181	0.62	37
HfNbTaTiZrW	3.286	3.376	2.74	22
HfNbTaTiZrMoW	3.273	3.348	2.29	22
WMoCrTiAl	3.178	3.154	0.76	21
TiNbTaZrMo	3.25	3.33	2.46	38
(TiVCr) ₉₅ W ₅	3.072	3.105	1.07	39
MoVW	3.11	3.05	1.93	40
CrMoVW	3.077	3.008	2.24	40
V _{2.5} Cr _{1.2} WMoCo _{0.04}	3.0594	3.1603	3.30	41

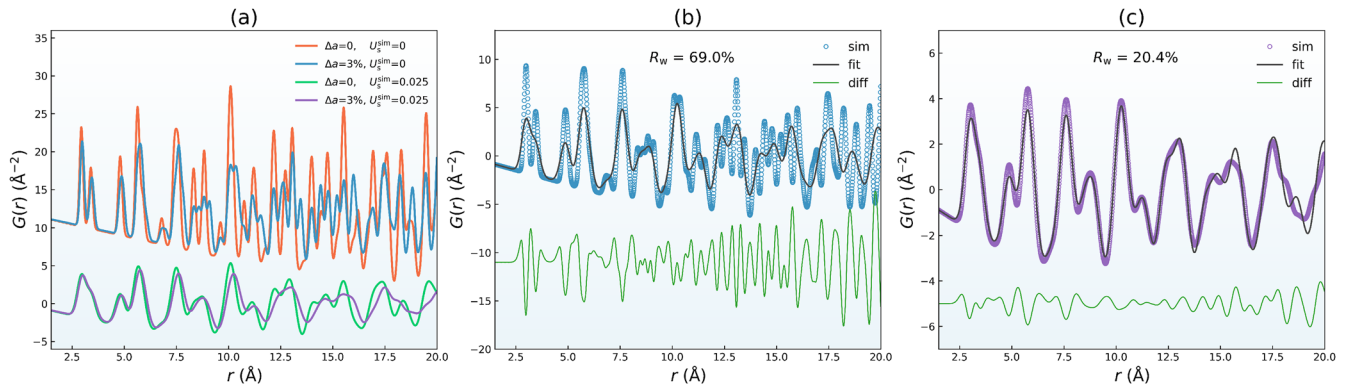


FIG. 2. (a) Extreme cases of simulated composite PDFs for $x_{ID} = 0.5$. (b) and (c) Single-phase fits to the PDFs corresponding to $\Delta a = 3\%$ and $U_s^{sim} = 0$, and $\Delta a = 3\%$ and $U_s^{sim} = 0.025$, respectively. R_w is the weighted profile R -factor from the fits.

small LLDs results in very poor fits [see Fig. 2(b)], and the resulting parameters derived cannot be expected to be physically meaningful.

The error, η , is plotted as a function of Δa and U_s^{sim} for different molar fractions in Figs. 3(a)–3(d), which provides insight into the reliability of using single-phase fitting to evaluate LLDs in segregated structures. By examining this figure, regions where the error is relatively small can be identified, and hence LLDs can be reliably extracted using a single-phase fit. Additionally, regions where the error is relatively high can be identified, and the resulting

values of LLDs should be treated with caution. In general, the error increases with increasing lattice parameter difference and decreasing magnitude of U_s^{sim} , as both of these characteristics will lead to more pronounced “separation” of the individual PDFs. As a result, the quality of the fit decreases with increasing Δa and decreasing U_s^{sim} , see Figs. 3(e)–3(h). However, it must be realized that η can still be large for low values of R_w , as R_w alone is not a sufficient metric to judge the accuracy. As the composite PDF progressively deviates from the qualitative shape of a single-phase PDF, the fitting

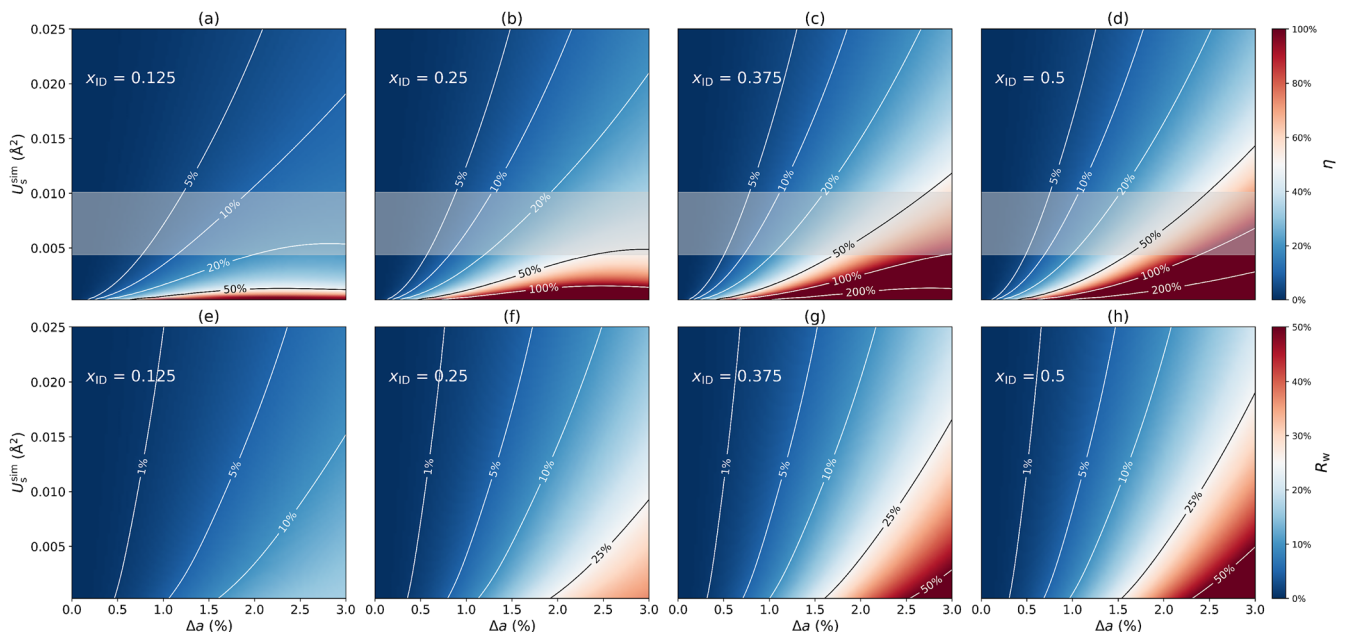


FIG. 3. (a)–(d) Error in the LLDs extracted from the single-phase fits, compared to the true simulated values. The color scale indicates the magnitude of the error, with red indicating large errors and blue indicating small errors. The white and black lines are iso- η contours. The translucent regions show the typical U_s range in RHEAs.²⁵ (e)–(h) R_w values of each fit, providing a first-order estimate of the goodness of the fit. The color scale indicates its magnitude, with red indicating large values (poor fits) while blue indicates small values (good fits). The white and black lines are iso- R_w contours.

parameters also lose their physical meaning since the model no longer accurately describes the data. This loss of physical meaning in the fitting parameters is the reason for the contradictory behavior seen for molar fractions below 0.5, where the rate of increase of η slows down at high values of Δa (above $\sim 2.5\%$) when the level of LLDs U_s^{sim} are small (below $\sim 0.01 \text{ \AA}^2$). The reduction in the rate of increase in the error does not signify a more accurate value of the LLDs but is rather an artifact from the fitting in a range where the model no longer describes the physical “reality”. In any real situation, care must be taken and the quality of the resulting fit must be judged before assigning physical meaning to fitting parameters and estimates of their accuracy.

The effect of molar fraction (x_{ID}) on the outcomes is relatively straightforward and intuitive. In Fig. 3, both the resulting values (η and R_w , respectively) increase with rising x_{ID} . A high x_{ID} value indicates a more balanced contribution from both phases rather than a dominant contribution from one phase. This equalization leads to a deviation from a purely single-phase scenario, thereby increasing the heterogeneity reflected in the composite PDF and, subsequently, the increased errors and worse fits observed during fitting.

Considering the static displacements range of most of the previously characterized RHEAs [$0.005 \lesssim U_s \lesssim 0.01 \text{ \AA}^2$, see the translucent regions in Figs. 3(a)–3(d)],²⁵ we observe that accurate estimates of U_s are reliably achieved for $\Delta a \lesssim 1\%$, where $\eta \lesssim 20\%$ and R_w is low. Although the reported values of Δa in Table II suggest that these criteria may not be frequently met, it is important to note that the table only includes a small subset of RHEAs for which Δa has been measured. Expanding the scope of high-resolution diffraction experiments to include a larger set of RHEAs will provide more definitive conclusions. Nevertheless, it is clear that if real-space fitting is to be used for the extraction of LLDs from PDFs, complementary measurements of Δa should be performed to help estimate the validity of the real-space fits.

Furthermore, it must be noted that the present study is idealized in the sense that all instrumental broadening effects are known, and sample-related broadening is neglected. In a real situation, the chemical gradients are expected to lead to the broadening of the peaks in reciprocal space due to gradual variations in lattice parameters across the regions. Such broadening will in turn have effects on the real-space peak widths.³⁴ While this can in many cases be neglected,²⁵ it should ideally be accounted for in more detailed simulations.

While outside the scope of this investigation, it is possible that the determination of U_{iso} from reciprocal-space refinements is a more suitable method in the presence of pronounced segregation. In reciprocal space, the Bragg peaks from both “phases” will have significant overlap, but as they will both undergo similar decay with diffraction angle due to the presence of LLDs, the refinement (which will attempt to capture the sum of the two peaks) will likely provide a reasonable estimate of U_{iso} even for large values of Δa . This, however, remains to be investigated in detail. Furthermore, it would be interesting to extend the analysis to fcc-structured HEAs, which generally show much smaller levels of LLDs.^{42,43} While small LLDs could be expected to be problematic in the current framework, the lattice parameter differences between segregated regions are also expected to be small due to the often very similar atomic sizes in typical fcc-structured HEAs. For small enough Δa , even very low values of U_s can be accurately captured, as seen in Figs. 3(a)–3(d).

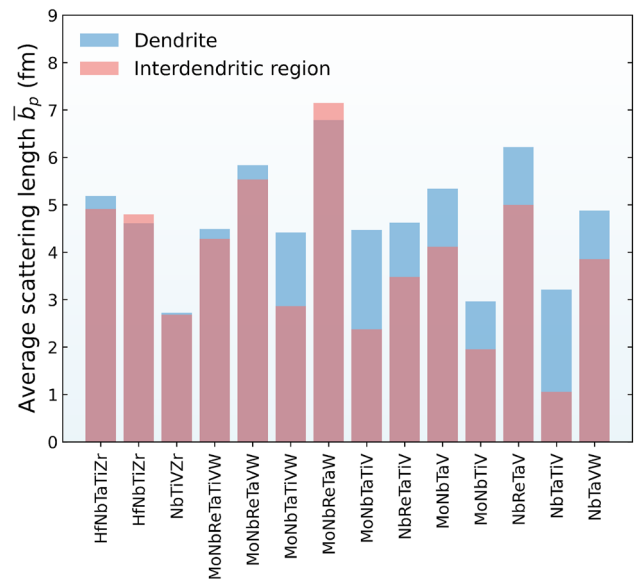


FIG. 4. The average neutron scattering lengths of dendrites and interdendritic regions from some bcc-structured RHEAs.¹⁵

Up to this point, we have assumed a negligible difference in the average scattering length between the different regions. However, RHEAs can exhibit relatively large differences due to the significant differences in chemistry.¹⁵ Although the difference in the average scattering length between the two regions is relatively small for most alloys, it can be as large as 70% in NbTaTiV and 50% in MoNbTaTiV (see Fig. 4). To investigate the effect of the average scattering length difference, we repeated the simulations using $\bar{b}_{\text{ID}} = 1.25\bar{b}_{\text{D}}$ ($\Delta\bar{b} = (\bar{b}_{\text{ID}} - \bar{b}_{\text{D}})/\bar{b}_{\text{D}} = 0.25$) and $\bar{b}_{\text{ID}} = 1.5\bar{b}_{\text{D}}$ ($\Delta\bar{b} = 0.5$) for all molar fractions.

The composite PDFs were fitted with a single-phase model, as before, and the resulting error estimate η is plotted in Fig. 5. The effect of the scattering length difference is very small for typical values of U_s , especially in the region $\Delta a \lesssim 1\%$ previously identified as reliable. Therefore, the presence of significant differences in the average scattering length between the regions does not affect the conclusions drawn, indicating that (in the region $\Delta a \lesssim 1\%$, and for typical values of U_s) such effects can be neglected in the analysis.

In summary, we quantitatively assess the error in the measurement of LLDs by simulating composite PDFs of segregated RHEAs. We demonstrate that using a single-phase model in small-box modeling to determine LLDs can lead to considerable errors in certain scenarios. Notably, the magnitude of these errors is influenced both by the degree of segregation and the differences in lattice parameters between the different regions. Generally, the errors grow with decreasing LLDs and increasing lattice parameter differences. The study concludes that for bcc-structured RHEAs, extracting LLDs from segregated structures using single-phase small-box analysis is reliable when lattice parameter differences are below around 1%. For larger differences, alternative methods such as large-box modeling or reciprocal-space refinements may offer better accuracy, but further investigation is needed to confirm this. In addition, we find that

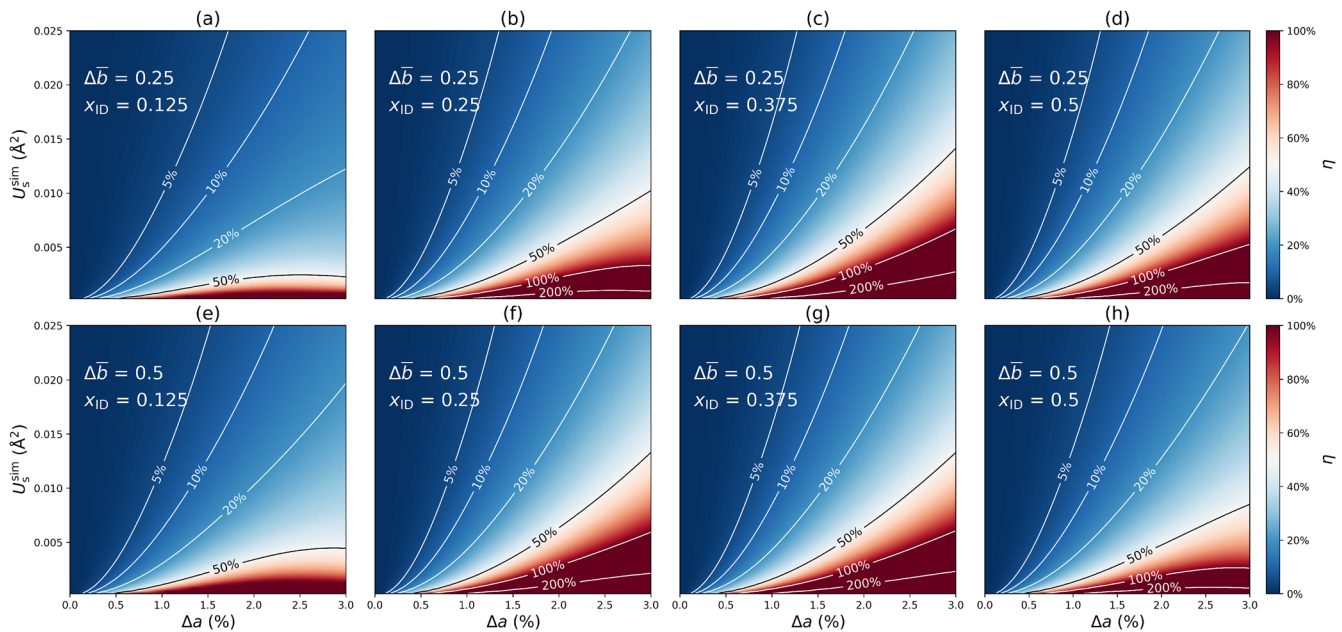


FIG. 5. Visualization of the impact of average scattering length difference and molar fraction on error determination. Similar simulations were performed as in Figs. 3(a)–3(d), with the scattering length of the interdendritic regions varied to differ by either (a)–(d) 25% or (e)–(h) 50% compared to the dendrites.

the impact of the scattering length difference on the accuracy of LLD determination is relatively subtle.

SUPPLEMENTARY MATERIAL

Schematic of the simulation and analysis workflow.

ACKNOWLEDGMENTS

This work was financially supported by Stiftelsen för Strategisk Forskning through the National Graduate School for Neutron Sciences (SwedNess): Grant No. GSn15-0008.

AUTHOR DECLARATIONS

Conflict of Interest

The authors have no conflicts to disclose.

Author Contributions

Yao Hu (胡尧): Conceptualization (supporting); Data curation (lead); Formal analysis (lead); Methodology (equal); Validation (equal); Visualization (lead); Writing – original draft (equal); Writing – review & editing (equal). **Sheng Guo:** Conceptualization (supporting); Formal analysis (supporting); Funding acquisition (equal); Project administration (equal); Supervision (equal); Writing – review & editing (equal). **Magnus Hörnqvist Colliander:** Conceptualization (equal); Formal analysis (supporting); Funding

acquisition (equal); Methodology (supporting); Project administration (equal); Supervision (equal); Writing – review & editing (equal).

DATA AVAILABILITY

The data that support the findings of this study are available from the corresponding author upon reasonable request.

REFERENCES

- J. W. Yeh, S. K. Chen, S. J. Lin, J. Y. Gan, T. S. Chin, T. T. Shun, C. H. Tsau, and S. Y. Chang, *Adv. Eng. Mater.* **6**, 299 (2004).
- B. Cantor, I. T. Chang, P. Knight, and A. J. Vincent, *Mater. Sci. Eng.: A* **375–377**, 213 (2004).
- E. P. George, D. Raabe, and R. O. Ritchie, *Nat. Rev. Mater.* **4**, 515 (2019).
- D. B. Miracle, *JOM* **69**, 2130 (2017).
- O. N. Senkov, D. B. Miracle, K. J. Chaput, and J. P. Couzinie, *J. Mater. Res.* **33**, 3092 (2018).
- C. Oses, C. Toher, and S. Curtarolo, *Nat. Rev. Mater.* **5**, 295 (2020).
- Y. Ma, Y. Ma, Q. Wang, S. Schweidler, M. Botros, T. Fu, H. Hahn, T. Brezesinski, and B. Breitung, *Energy Environ. Sci.* **14**, 2883 (2021).
- Y. Sun and S. Dai, *Sci. Adv.* **7**, 1 (2021).
- Z. Wang, Q. Fang, J. Li, B. Liu, and Y. Liu, *J. Mater. Sci. Technol.* **34**, 349 (2018).
- C. Lee, Y. Chou, G. Kim, M. C. Gao, K. An, J. Brechtel, C. Zhang, W. Chen, J. D. Poplawsky, G. Song, Y. Ren, Y. C. Chou, and P. K. Liaw, *Adv. Mater.* **32**, 2004029 (2020).
- P. Thirathipiwat, S. Sato, G. Song, J. Bednarcik, K. Nielsch, J. Jung, and J. Han, *Scr. Mater.* **210**, 114470 (2022).
- G. D. Samolyuk, Y. N. Osetsky, G. M. Stocks, and J. R. Morris, *Phys. Rev. Lett.* **126**, 025501 (2021).

- ¹³T. Egami and S. J. L. Billinge, *Underneath the Bragg Peaks: Structural Analysis of Complex Materials*, 2nd ed. (Elsevier, 2012).
- ¹⁴W. Guo, W. Dmowski, J.-Y. Noh, P. Rack, P. K. Liaw, and T. Egami, *Metall. Mater. Trans. A* **44**, 1994 (2013).
- ¹⁵Y. Tong, S. Zhao, H. Bei, T. Egami, Y. Zhang, and F. Zhang, *Acta Mater.* **183**, 172 (2020).
- ¹⁶F. Meng, W. Zhang, Z. Zhou, R. Sheng, A. C. Chuang, C. Wu, H. Huang, S. Zhang, H. Zhang, L. Zhu, L. Jiang, P. K. Liaw, S. Chen, and Y. Tong, *Scr. Mater.* **203**, 114104 (2021).
- ¹⁷L. R. Owen, H. J. Stone, and H. Y. Playford, *Acta Mater.* **170**, 38 (2019).
- ¹⁸L. R. Owen and N. G. Jones, *Scr. Mater.* **187**, 428 (2020).
- ¹⁹O. N. Senkov, G. B. Wilks, D. B. Miracle, C. P. Chuang, and P. K. Liaw, *Intermetallics* **18**, 1758 (2010).
- ²⁰A. Manzoni, H. Daoud, R. Völkl, U. Glatzel, and N. Wanderka, *Ultramicroscopy* **132**, 212 (2013).
- ²¹B. Gorr, M. Azim, H. J. Christ, H. Chen, D. V. Szabo, A. Kauffmann, and M. Heilmair, *Metall. Mater. Trans. A* **47**, 961 (2016).
- ²²M. Wang, Z. Ma, Z. Xu, and X. Cheng, *J. Alloys Compd.* **803**, 778 (2019).
- ²³H. Song, F. Tian, Q. M. Hu, L. Vitos, Y. Wang, J. Shen, and N. Chen, *Phys. Rev. Mater.* **1**, 23404 (2017).
- ²⁴Y. Y. Zhao, Z. F. Lei, Z. P. Lu, J. C. Huang, and T. G. Nieh, *Mater. Res. Lett.* **7**, 340 (2019).
- ²⁵Y. Hu, L. R. Owen, H. Y. Playford, A. Edgren, S. Guo, and M. H. Colliander, *Phys. Rev. Mater.* **8**, 083602 (2024).
- ²⁶C. L. Farrow, P. Juhas, J. W. Liu, D. Bryndin, E. S. Božin, J. Bloch, T. Proffen, and S. J. Billinge, *J. Phys.: Condens. Matter* **19**, 335219 (2007).
- ²⁷P. Juhas, C. L. Farrow, X. Yang, K. R. Knox, and S. J. Billinge, *Acta Crystallogr., Sect. A: Found. Adv.* **71**, 562 (2015).
- ²⁸W. A. Ślawiński, *J. Appl. Crystallogr.* **51**, 919 (2018).
- ²⁹D. A. Keen, *J. Appl. Crystallogr.* **34**, 172 (2001).
- ³⁰P. F. Peterson and D. A. Keen, *J. Appl. Crystallogr.* **54**, 1542 (2021).
- ³¹I.-K. Jeong, R. H. Heffner, M. J. Graf, and S. J. L. Billinge, *Phys. Rev. B* **67**, 104301 (2003).
- ³²D. A. Keen, *Crystallogr. Rev.* **26**, 143 (2020).
- ³³X. Qiu, E. S. Božin, P. Juhas, T. Proffen, and S. J. Billinge, *J. Appl. Crystallogr.* **37**, 110 (2004).
- ³⁴I. K. Jeong, M. J. Graf, and R. H. Heffner, *J. Appl. Crystallogr.* **38**, 55 (2005).
- ³⁵D. Olds, C. N. Saunders, M. Peters, T. Proffen, J. Neufeind, and K. Page, *Acta Crystallogr., Sect. A: Found. Adv.* **74**, 293 (2018).
- ³⁶J. Beyer, N. Roth, and B. Brummerstedt Iversen, *Acta Crystallogr., Sect. A: Found. Adv.* **78**, 10 (2022).
- ³⁷F. Lukac, M. Dudr, R. Musalek, J. Klecka, J. Cinert, J. Cizek, T. Chraska, J. Cizek, O. Melikhova, J. Kuriplach, J. Zyka, and J. Malek, *J. Mater. Res.* **33**, 3247 (2018).
- ³⁸M. Todai, T. Nagase, T. Hori, A. Matsugaki, A. Sekita, and T. Nakano, *Scr. Mater.* **129**, 65 (2017).
- ³⁹C. Li, S. Chen, H. Tang, J. Zhang, J. Liu, and Y. Wu, *Int. J. Refract. Met. Hard Mater.* **116**, 106329 (2023).
- ⁴⁰D. Ikeuchi, D. King, K. Laws, A. Knowles, R. Aughterson, G. Lumpkin, and E. Obbard, *Scr. Mater.* **158**, 141 (2019).
- ⁴¹D. Patel, M. D. Richardson, B. Jim, S. Akhmaliev, R. Goodall, and A. S. Gandy, *J. Nucl. Mater.* **531**, 152005 (2020).
- ⁴²L. R. Owen, E. J. Pickering, H. Y. Playford, H. J. Stone, M. G. Tucker, and N. G. Jones, *Acta Mater.* **122**, 11 (2017).
- ⁴³L. Owen, N. Jones, H. Stone, and H. Playford, *Acta Mater.* **262**, 119164 (2024).